2011 International Symposium on Nonlinear Theory and its Applications
NOLTA2011, Kobe, Japan, September 4-7, 2011

# Nonlinear Koopman Mode Analysis and Power System Swing Stability

Yoshihiko Susuki† and Igor Mezić‡

†Department of Electrical Engineering
Kyoto University
Katsura, Kyoto 615–8510 Japan
susuki@ieee.org

‡Department of Mechanical Engineering
University of California, Santa Barbara
CA 93106–5070 United States
mezic@engineering.ucsb.edu

**Abstract**—We review the Koopman Mode Analysis (KMA) for nonlinear spatio-temporal dynamics and report its application to power system analysis. KMA is a natural extension of the traditional linear mode analysis and is based on spectral theory of dynamical systems. For a given data on highly nonlinear dynamics, it gives a set of spatial modes of oscillation with single frequency. KMA is used for analysis of swing dynamics in a group of synchronous machines that are of vital importance for planning and operation of electric power systems.

## 1. Introduction

Mode analysis plays an important role in power system analysis and control. Conventional methods are based on linear system dynamics and have been traditionally applied to power system studies. Due to nonlinear dynamics with multi-scale and multi-physics in power systems, the linear mode analysis does not often give a clear solution for power system analysis and control. A new approach to this is strongly required, especially in future power grids with emphasis on accurate monitoring, analysis, and control of physical power systems.

In the farmer part of this paper, we review the *Koopman Mode Analysis* (KMA) that is developed in [1]. KMA is based on operator theory of dynamical systems and gives a natural extension of the standard linear oscillatory mode analysis. Koopman pioneered the use of linear operators on Hilbert space to analyze nonlinear Hamiltonian systems by introducing the so-called *Koopman operator* and studying its spectrum [2]. This linear, infinite-dimensional operator is defined for arbitrary nonlinear dynamical systems [3]. In [1] the author showed via spectral analysis of the Koopman operator that single-frequency modes can be embedded in highly nonlinear, spatiotemporal dynamics. In Sec. 2 we summarize the KMA with emphasis on numerical computation.

In the latter part of this paper (Sec. 3), we present an application of the KMA to swing dynamics in a multi-machine power system. Swing dynamics of synchronous machines are of vital importance for power system stability and control [4]. The so-called short-term swings are associated with nonlinear electromechanical oscillations of synchronous machines coupled via a transmission network. Nonlinear phenomena are reported in this subject [5, 6, 7]. We apply the KMA to coupled swing dynamics in the New England test system [8] and show that the KMA can extract a set of spatial modes of oscillation with single frequency. The contents are based on [9] and obtained with a slightly different set of parameters.

## 2. Nonlinear Koopman Mode

We introduce the theory of Koopman operator and Koopman mode for nonlinear dynamical systems. The contents here are based on [9]. Consider a discrete-time, nonlinear dynamical system evolving on a smooth, finite-dimensional manifold $M$, given by

$$\boldsymbol{x}_{k+1} \quad = \quad \boldsymbol{F}(\boldsymbol{x}_k), \tag{1}$$

where $\boldsymbol{x} \in M$ is the state belonging to $M$, and $\boldsymbol{F} : M \to M$ is a nonlinear vector-valued mapping. The *Koopman operator* is a linear operator $\mathcal{U}$ that acts on scalar-valued functions defined on $M$ in the following manner: for $g : M \to \mathbb{R}$,

$$\mathcal{U}g(\boldsymbol{x}) \quad = \quad g(\boldsymbol{F}(\boldsymbol{x})). \tag{2}$$

Although the dynamical system is nonlinear and evolves on the finite-dimensional space, the Koopman operator $\mathcal{U}$ is linear and infinite-dimensional. The eigenfunctions and eigenvalues of $\mathcal{U}$ are defined as follows: for functions $\varphi_j : M \to \mathbb{C}$ and constants $\lambda_j \in \mathbb{C}$,

$$\mathcal{U}\varphi_j(\boldsymbol{x}) \quad = \quad \lambda_j\varphi_j(\boldsymbol{x}), \quad j = 1, 2, \ldots \tag{3}$$

In the following, we refer to $\varphi_j$ as *Koopman eigenfunctions* of $\mathcal{U}$ and to $\lambda_j$ as the associated *Koopman Eigenvalues* (KEs).

The idea in [1, 10] is to analyze nonlinear dynamics governed by (1), using the linear operator $\mathcal{U}$ and its eigenstructure. To this end, consider a vector-valued *observable* $\boldsymbol{g} : M \to \mathbb{R}^p$. For example, if $\boldsymbol{x} \in M$ contains the full information about system dynamics at a particular time, $\boldsymbol{g}(\boldsymbol{x})$ is a vector of any measured quantities of interest, such as frequencies and voltages measured at various points in a power system. In [1] the author shows that if the dynamical system (1) possesses a smooth invariant measure, or the initial condition $\boldsymbol{x}_0$ of (1) is on any attractor, then $\boldsymbol{g}(\boldsymbol{x}_k)$ is exactly represented as

$$\boldsymbol{g}(\boldsymbol{x}_k) = \sum_{j=1}^{\infty} \lambda_j^k \varphi_j(\boldsymbol{x}_0)\boldsymbol{v}_j + \begin{bmatrix} \int_0^{2\pi} \mathrm{e}^{\mathrm{i}k\theta}\mathrm{d}E(\theta)g_1(\boldsymbol{x}_0) \\ \vdots \\ \int_0^{2\pi} \mathrm{e}^{\mathrm{i}k\theta}\mathrm{d}E(\theta)g_p(\boldsymbol{x}_0) \end{bmatrix}, \tag{4}$$

where $g_i(\boldsymbol{x})$ is the $i$-th element of $\boldsymbol{g}(\boldsymbol{x})$, and $E(\theta)$ is a continuous, complex spectral measure. The modulus of KEs $\lambda_i$ is identically one, because $\mathcal{U}$ is a unitary operator in

the above situation [3]. In (4) we refer to the vectors $\boldsymbol{v}_j$ as *Koopman Modes* (KMs) of the system (1), corresponding to $\boldsymbol{g}$. On the right-hand side of (4), the first term represents the contribution of KEs (namely, point spectra of $\mathcal{U}$) to the time evolution $\{\boldsymbol{g}(\boldsymbol{x}_k)\}$ and describes the average and quasi-periodic parts of $\{\boldsymbol{g}(\boldsymbol{x}_k)\}$. On the other hand, the last term represents the contribution of continuous spectrum of $\mathcal{U}$ and describes the aperiodic part of $\{\boldsymbol{g}(\boldsymbol{x}_k)\}$. Hence, if the dynamics observed in (1) have no continuous spectrum in frequency domain (practical experience in power system analysis suggests this situation), then the dynamics are simply represented as

$$\boldsymbol{g}(\boldsymbol{x}_k) \quad = \quad \sum_{j=1}^{\infty} \lambda_j^k \varphi_j(\boldsymbol{x}_0)\boldsymbol{v}_j. \tag{5}$$

In [1, 10], the authors show that the terms $\varphi_j(\boldsymbol{x}_0)\boldsymbol{v}_j$ are defined and computed with a projection operation associated with $\mathcal{U}$ applied to $\boldsymbol{g}(\boldsymbol{x})$. Define a family of linear operators $\mathcal{P}^\nu$: for $g : M \to \mathbb{R}$,

$$\mathcal{P}^\nu g(\boldsymbol{x}_0) \quad = \quad \lim_{n\to\infty} \frac{1}{n} \sum_{k=0}^{n-1} \mathrm{e}^{-\mathrm{i}2\pi k\nu} g(\boldsymbol{x}_k), \tag{6}$$

where $\nu \in [-1/2, 1/2)$. When the initial condition $\boldsymbol{x}_0$ is on an attractor of (1), a nonzero $\mathcal{P}^\nu$ is the orthogonal projection operator onto the eigenspace of $\mathcal{U}$ associated with the KE $\lambda = \mathrm{e}^{\mathrm{i}2\pi\nu}$. The projections of the $p$ components $g_1, \ldots, g_p$ of $\boldsymbol{g}$ on the $j$-th eigenspace are obtained:

$$\begin{bmatrix} \mathcal{P}^{\nu_j} g_1(\boldsymbol{x}_0) \\ \vdots \\ \mathcal{P}^{\nu_j} g_p(\boldsymbol{x}_0) \end{bmatrix} \quad = \quad \varphi_j(\boldsymbol{x}_0)\boldsymbol{v}_j, \tag{7}$$

where $\nu_j = \mathrm{Im}[\ln \lambda_j]/2\pi$. This formula (7) associates $\varphi_j(\boldsymbol{x}_0)\boldsymbol{v}_j$ with the projection operation based on the operator $\mathcal{P}^\nu$. The left-hand sides of (7) are just the Fourier transforms of the observations $\{\boldsymbol{g}(\boldsymbol{x}_0), \boldsymbol{g}(\boldsymbol{x}_1), \ldots\}$, and the terms $\varphi_j(\boldsymbol{x}_0)\boldsymbol{v}_j$ can be computed.

Until now we assume that the dynamics of (1) are on an attractor. Even if this is not the case, that is, we consider dynamics off attractors or transient dynamics of (1), the KM modes oscillate with a single frequency. If each of the $p$ components of $\boldsymbol{g}$ lies within the span of eigenfunctions $\varphi_j$, then, as in [11], we may expand the vector-valued $\boldsymbol{g}$ in terms of these eigenfunctions as

$$\boldsymbol{g}(\boldsymbol{x}) \quad = \quad \sum_{j=1}^{\infty} \varphi_j(\boldsymbol{x})\boldsymbol{v}_j, \tag{8}$$

where $\boldsymbol{v}_j$ are regarded as the (vector) coefficients in the expansion. The time evolution $\{\boldsymbol{g}(\boldsymbol{x}_k)\}$ starting at $\boldsymbol{g}(\boldsymbol{x}_0)$ is identically given by (5):

$$\begin{aligned} \boldsymbol{g}(\boldsymbol{x}_k) \quad &= \quad \sum_{j=1}^{\infty} \varphi_j(\boldsymbol{x}_k)\boldsymbol{v}_j \quad = \quad \sum_{j=1}^{\infty} \mathcal{U}^k \varphi_j(\boldsymbol{x}_0)\boldsymbol{v}_j \\ &= \quad \sum_{j=1}^{\infty} \lambda_j^k \varphi_j(\boldsymbol{x}_0)\boldsymbol{v}_j. \end{aligned} \tag{9}$$

Thus we can refer to $\boldsymbol{v}_j$ as the KM which oscillates with a single frequency. If the dynamics observed here have only a finite number of discrete spectra in frequency domain, then we can expect that the expansion gives a good approximation of the dynamics. In this way, the KE $\lambda_j$ characterizes the temporal behavior of the corresponding KM $\boldsymbol{v}_j$: the phase of $\lambda_j$ determines its frequency, and the magnitude determines the growth or decay rate.

While the general Fourier analysis allows us to compute KMs on an attractor, off attractors the KMs as well as KEs can be computed using the Arnoldi algorithm [11]. Suppose that we have a sequence of $N + 1$ observations $\{\boldsymbol{g}(\boldsymbol{x}_0), \ldots, \boldsymbol{g}(\boldsymbol{x}_N)\}$. Let us define the *empirical Ritz values* $\tilde{\lambda}_j$ and *empirical Ritz vectors* $\tilde{\boldsymbol{v}}_j$ of this sequence by using the following algorithm:

(i) Define constants $c_j$ such that for vector $\boldsymbol{r}$ satisfying $\boldsymbol{r} \perp \mathrm{span}\{\boldsymbol{g}(\boldsymbol{x}_0), \ldots, \boldsymbol{g}(\boldsymbol{x}_{N-1})\}$,

$$\boldsymbol{r} \quad = \quad \boldsymbol{g}(\boldsymbol{x}_N) - \sum_{j=0}^{N-1} c_j \boldsymbol{g}(\boldsymbol{x}_j). \tag{10}$$

(ii) Define the companion matrix $\mathsf{C}$ as

$$\mathsf{C} \quad = \quad \begin{bmatrix} 0 & 0 & \cdots & 0 & c_0 \\ 1 & 0 & \cdots & 0 & c_1 \\ 0 & 1 & \cdots & 0 & c_2 \\ \vdots & \vdots & \ddots & \vdots & \vdots \\ 0 & 0 & \cdots & 1 & c_{N-1} \end{bmatrix}. \tag{11}$$

and find its $N$ eigenvalues $\tilde{\lambda}_1, \ldots, \tilde{\lambda}_N$.

(iii) Define the Vandermonde matrix $\mathsf{T}$ using $\tilde{\lambda}_j$ as

$$\mathsf{T} \quad = \quad \begin{bmatrix} 1 & \tilde{\lambda}_1 & \tilde{\lambda}_1^2 & \cdots & \tilde{\lambda}_1^{N-1} \\ 1 & \tilde{\lambda}_2 & \tilde{\lambda}_2^2 & \cdots & \tilde{\lambda}_2^{N-1} \\ \vdots & \vdots & \vdots & \ddots & \vdots \\ 1 & \tilde{\lambda}_N & \tilde{\lambda}_N^2 & \cdots & \tilde{\lambda}_N^{N-1} \end{bmatrix}. \tag{12}$$

(iv) Define $\tilde{\boldsymbol{v}}_j$ to be the columns of $\mathsf{V} = [\boldsymbol{g}(\boldsymbol{x}_0)\, \boldsymbol{g}(\boldsymbol{x}_1) \cdots \boldsymbol{g}(\boldsymbol{x}_{N-1})]\mathsf{T}^{-1}$.

Then, we have the following equations that are originally derived in [11]:

$$\boldsymbol{g}(\boldsymbol{x}_k) = \sum_{j=1}^{N} \tilde{\lambda}_j^k \tilde{\boldsymbol{v}}_j, \quad \boldsymbol{g}(\boldsymbol{x}_N) = \sum_{j=1}^{N} \tilde{\lambda}_j^N \tilde{\boldsymbol{v}}_j + \boldsymbol{r}, \tag{13}$$

where $k = 0 \ldots, N-1$. Comparing with (5), the empirical Ritz values $\tilde{\lambda}_j$ and vectors $\tilde{\boldsymbol{v}}_j$ behave precisely in the same manner as the KEs $\lambda_j$ and the terms $\varphi_j(\boldsymbol{x}_0)\boldsymbol{v}_j$ of Koopman eigenfunctions and KMs, but for the finite sum (13) instead of the infinite sum (5).

## 3. Application to Power System Analysis

In this section, we apply the KMA to coupled swing dynamics in the New England (NE) 39-bus test system. The

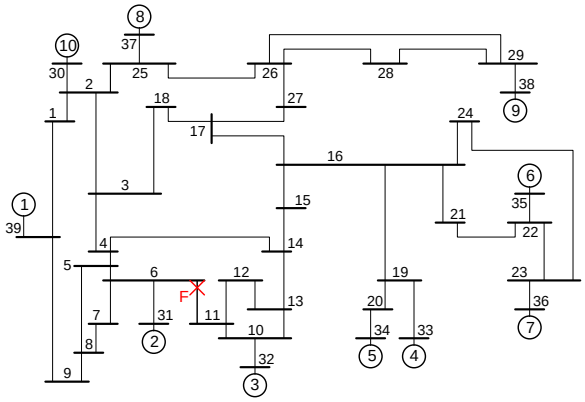

Figure 1: The New England 39-bus test system [8]

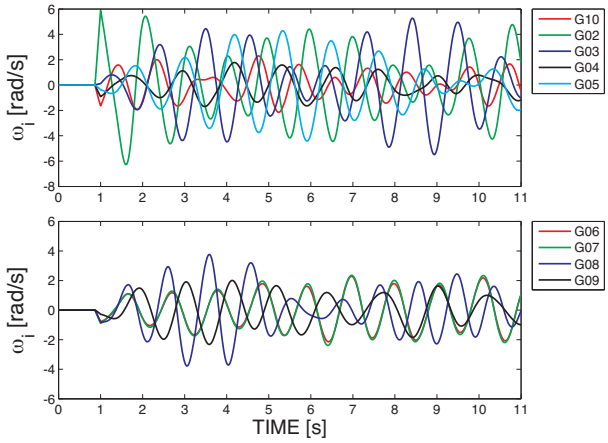


Figure 2: Coupled swing dynamics of the 9 generators in the New England 39-bus test system

NE system is shown in Fig. 1 and is a well-known benchmark system for power system studies [8]. The system contains the 10 generation units (equivalent 10 synchronous generators, circled numbers in the figure), the 39 buses, and AC transmission lines. Most of the buses have constant active and reactive power loads. Assume that bus 39 is the infinite bus.

Figure 2 shows an example of coupled swing dynamics of generators 2–10 in the NE system. The dynamics are obtained with numerical integration of the nonlinear swing equations [4] for the system (see [9]). All numerical simulations discussed in this section were performed using MATLAB. The parameters of the equations are basically fixed using the nominal values in [8]. We suppose that the magnitudes of the line reactances are 30 times larger than in [8], that the mechanical input power to the generators and constant power loads are 50% at their ratings, and the damping coefficients of the generators are uniformly 0.005. Under the settings, we investigate nonlinear swing dynamics under a heavily lossy network, light loading conditions, and small damping that may appear in a low-voltage distribution network. We use the following fault condition: each generator operates at a steady condition at $t = 0$ s. Then a three-phase fault happens at point F near bus 6 at $t = 1\,\text{s} - 8/(60\,\text{Hz}) \approx 0.87$ s, and line 6–11 trips at $t = 1$ s. The fault duration is 8 cycles of a 60-Hz sinusoidal wave. The fault is simulated by adding a small impedance $(10^{-7}\text{i})$

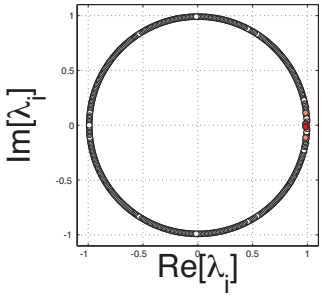


Figure 3: Koopman eigenvalues (empirical Ritz values) $\tilde{\lambda}_j$ obtained with the Arnoldi-based algorithm. The color varies smoothly from red to white, depending on the norm of the corresponding mode.

Table 1: Numerical results on the Koopman modes

| Mode | $\lvert\tilde{\lambda}_j\rvert$ | $\tilde{f}_j$ / Hz | $\lVert\tilde{\boldsymbol{v}}_j\rVert$ |
|---|---|---|---|
| 1 | 1.0002 | 1.2921 | $4.3358 \times 10^{-1}$ |
| **2** | $9.9911 \times 10^{-1}$ | $3.9045 \times 10^{-1}$ | $6.2621 \times 10^{-1}$ |
| **3** | $9.9813 \times 10^{-1}$ | $9.8397 \times 10^{-1}$ | 4.8215 |
| 4 | $9.9807 \times 10^{-1}$ | 1.7139 | $2.1461 \times 10^{-1}$ |
| 5 | $9.9760 \times 10^{-1}$ | 1.5060 | $4.2192 \times 10^{-1}$ |
| 6 | $9.9659 \times 10^{-1}$ | $7.1001 \times 10^{-1}$ | 2.2057 |
| **7** | $9.9653 \times 10^{-1}$ | $7.9905 \times 10^{-1}$ | 6.3235 |

between bus 6 and the ground. In the figure, $\omega_i$ denotes the deviation of rotor speed in generator $i$ relative to the system angular frequency ($2\pi \times 60$ Hz). After clearing the fault at $t = 1$ s, complicated swings happen in the 9 generators. They contain more than one frequency, that is, behave in a multiple-periodic manner during the duration. Generators 2 and 3 have large swings because they are electrically close to the location of the local fault. This figure shows that all of the 9 machines respond to the local fault in an oscillatory manner.

Now we compute the KEs and KMs (the empirical Ritz values $\tilde{\lambda}_j$ and associated vectors $\tilde{\boldsymbol{v}}_j$) using the Arnoldi-based algorithm. As a sequence of sampled observations $\{\boldsymbol{g}(\boldsymbol{x}_k)\}_{k=0}^{N}$, we use the simulation output shown in Fig. 2 that extracts the vector of rotor speed deviations $\{\boldsymbol{\omega}(kT + 1\,\text{s})\}_{k=0}^{N}$, where the uniform sampling period $T = 1/(50\,\text{Hz})$ and the number of samples $N + 1 = 501$. Here we use $\boldsymbol{\omega} = (\omega_{10}, \omega_2, \ldots, \omega_9)^{\mathsf{T}}$, where $\mathsf{T}$ indicates transpose in vectors. The choice of the observations has a clear physical meaning in power systems: one measures rotor speeds or frequencies for every generation plant that are directly related to kinetic energy stored in the generators. For computation, the implementation of Step (i) in the computation algorithm is described in [9].

Figure 3 shows the KEs (empirical Ritz values) $\tilde{\lambda}_j$. The norm of $\boldsymbol{r}$ in Step (i) is of order $10^{-13}$. Many KMs are obtained and are close to the unit circle $|\tilde{\lambda}_j| = 1$. Now let us focus on KMs that have both large growth rates $|\tilde{\lambda}_j|$ and large norms of $\tilde{\boldsymbol{v}}_j$. Such modes represent sustained swing components for the time duration and have dominant magnitudes in the outputs. Tab. 1 shows numerical results on KEs and KMs, which we call Mode 1 to Mode 7. The norm for Mode $j$ is defined as $\|\tilde{\boldsymbol{v}}_j\| = \sqrt{\tilde{\boldsymbol{v}}_j^{\mathsf{T}}\tilde{\boldsymbol{v}}_j}$. The order of KMs in Tab. 1 is based on the magnitudes of growth rates, $|\tilde{\lambda}_j|$. Now we pick up Mode 2, Mode 3 and Mode 7 that have large norms in the table. Mode 6 has a large norm, too. But its frequency is close to Mode 7, and hence we do not consider the mode. Fig. 4 shows the vectors of the three KMs $\tilde{\boldsymbol{v}}_j$ ($j = 2, 3, 7$). For the KMs, the associated amplitude coefficients $A_{ji} := |\tilde{v}_{ji}|$ and initial phases $\alpha_{ji} := \text{Arg}(\tilde{v}_{ji})$

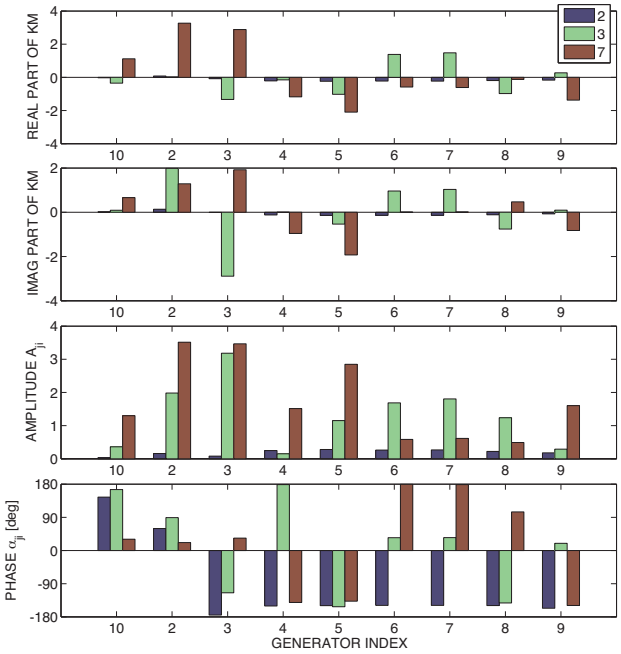


Figure 4: Koopman modes $\tilde{\boldsymbol{v}}_j$ ($j = 2, 3, 7$) in Table 1

($i = 2, \ldots, 10$) are also shown ($\tilde{v}_{ji}$ denotes the $i$-the entry of $\tilde{\boldsymbol{v}}_j$).[1] Mode 2 implies a coherent swing with a low frequency in generators 4–9. On the other hand, Mode 3 has a high peak of amplitudes at generator 3. Mode 7 have high peaks of amplitudes at generators 2 and 3. These modes contribute localized swings at these generators that are electrically close to the location of the local fault. Fig. 5 shows the modal dynamics for Mode $j$, denoted by $\boldsymbol{g}^j(\boldsymbol{x}_k)$:

$$\boldsymbol{g}^j(\boldsymbol{x}_k) \quad = \quad \tilde{\lambda}_j^k \tilde{\boldsymbol{v}}_j + (\tilde{\lambda}_j^{\mathrm{c}})^k \tilde{\boldsymbol{v}}_j^{\mathrm{c}}, \tag{14}$$

where $\tilde{\lambda}_j^{\mathrm{c}}$ (or $\tilde{\boldsymbol{v}}_j^{\mathrm{c}}$) denotes the complex-conjugate of $\tilde{\lambda}_j$ (or $\tilde{\boldsymbol{v}}_j$). Here we implicitly assume that Mode $j$ has none-zero imaginary part in the KE. Each KM contains single frequency by construction. The swing of Mode 2, namely the coherent swing of generators 4–9, is not dominant energetically. However, it is reported in [12] that such a coherent mode governs a phenomenon of global swing instabilities in the NE system. The dynamically relevant but small-energy mode can be detected with the KMA. Also, the KMA decouples frequency information more clearly than proper orthogonal decomposition (see [9, 11]). In this way, the coupled swing dynamics in the NE system are decomposed into a set of KMs, namely, spatial modes of oscillation with single frequency.

**Acknowledgements** We thank Prof. T. Hikihara (Kyoto University) for his valuable suggestions and warm encouragements. This work was supported in part by JSPS Postdoctoral Fellowships for Research Abroad, in part by NICT Project ICE-IT, and in part by Grant-in-Aid for Young Scientists (B) 23760390, MEXT Japan.

[1] In the previous paper [9] we use another definition of the initial phase $\alpha_{ji} := \tan^{-1}(\mathrm{Im}[\tilde{v}_{ji}]/\mathrm{Re}[\tilde{v}_{ji}])$. In case that the range of $\tan^{-1}$ is assumed to be $[-\pi/2, \pi/2]$, the previous definition may not give $\mathrm{Arg}(\tilde{v}_{ji}) \in [-\pi, \pi)$, that is, precise phase information. The current definition is better in this case.

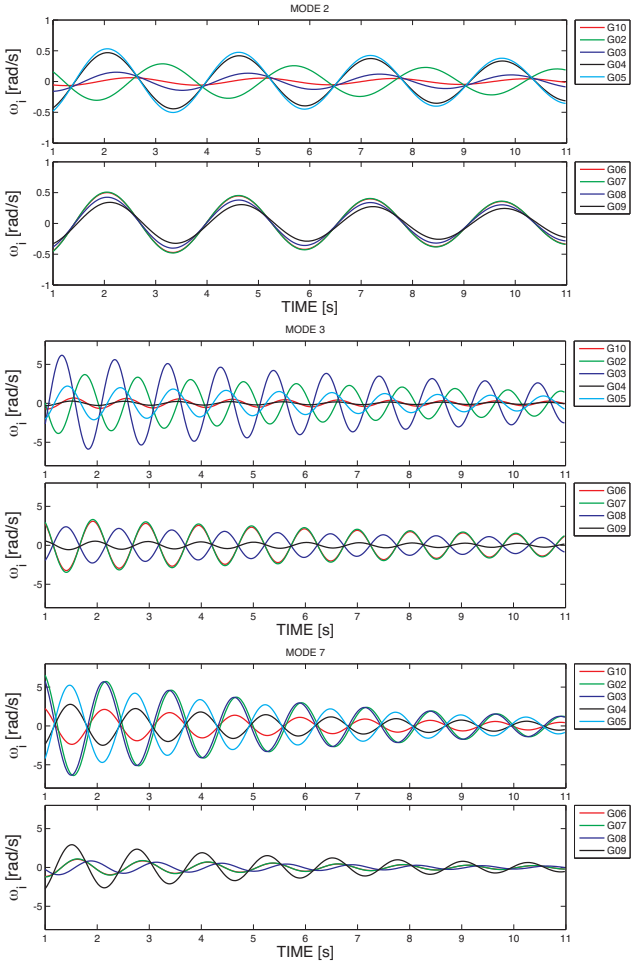


Figure 5: Modal dynamics (14) of the Koopman modes $\tilde{\boldsymbol{v}}_j$ ($j = 2, 3, 7$)

## References

[1] I. Mezić, *Nonlinear Dyn.*, vol.41, pp.309–325 (2005).
[2] B. O. Koopman, *P. Natl. Acad. Sci. USA*, vol.17, no.5, pp.315–318 (1931).
[3] A. Lasota and M. C. Mackey, *Chaos, Fractals, and Noise*, 2nd ed. (Springer-Verlag, 1994).
[4] P. Kundur, *Power System Stability and Control* (McGraw-Hill, 1994).
[5] N. Kopell and R. B. Washburn, Jr., *IEEE T. Circuits Syst.*, vol.CAS-29, no.11, pp.738–746 (1982).
[6] F. M. A. Salam, J. E. Marsden, and P. P. Varaiya, *IEEE T. Circuits Syst.*, vol.CAS-31, no.8, pp.673–688 (1984).
[7] H. -D. Chiang, C. -W. Liu, P. P. Varaiya, F. F. Wu, and M. G. Lauby, *IEEE T. Power Syst.*, vol.8, no.4, pp.1407–1417 (1993).
[8] M. A. Pai, *Energy Function Analysis for Power System Stability* (Academic Pub., 1989).
[9] Y. Susuki and I. Mezić, *IEEE T. Power Syst.* (2011; published online. doi:10.1109/TPWRS.2010.2103369); *Proc. IEEE PES General Meeting*, Minneapolis, United States, July (2010).
[10] I. Mezić and A. Banaszuk, *Physica D*, vol.197, pp.101–133 (2004).
[11] C. Rowley, I. Mezić, S. Bagheri, P. Schlatter, and D. S. Henningson, *J. Fluid Mech.*, vol.641, pp.115–127 (2009).
[12] Y. Susuki, I. Mezić, and T. Hikihara, *J. Nonlinear Sci.* (2011; published online. doi:10.1007/s00332-010-9087-5).